ACS OMEGA

Open Access

http://pubs.acs.org/journal/acsodf

Article

Enhanced Ion Solvation and Conductivity in Lithium-Ion Electrolytes via Tailored EMC-TMS Solvent Mixtures: A Molecular Dynamics Study

Jitti Kasemchainan, Siriporn Teeraburanapong, and Manaswee Suttipong*

Cite This: *ACS Omega* 2025, 10, 2141−2149

Read Online

ACCESS | Metrics & More | Article Recommendations | Supporting Information

ABSTRACT: The development of stable, high-performance electrolytes is essential to addressing the safety concerns and limited lifespan caused by the thermal and chemical instability of traditional organic carbonate-based electrolytes in lithium-ion batteries (LIBs). This study examined the potential of mixed solvent systems, specifically ethyl methyl carbonate (EMC) and tetramethylene sulfone (TMS), to modify ion solvation and improve ionic conductivity in LIB electrolytes. Through molecular dynamics simulations, we investigated the solvation structure and transport properties of lithium ions (Li^+) in these solvent environments. The inclusion of TMS altered the solvation structure, with TMS molecules preferentially coordinating with Li^+ ions, displacing PF_6^- anions and reducing their electrostatic interference. Our results demonstrated a synergistic interaction between EMC and TMS, where an EMC/TMS ratio of 1:2 led to a significant improvement in ionic conductivity, reaching 0.91 mS/cm, with a corresponding Li^+ transference number of 0.40. These findings provide key insights into the molecular-level interaction governing electrolyte behavior, offering guidance for the design of future solvent mixtures to improve the safety and efficiency of LIBs.

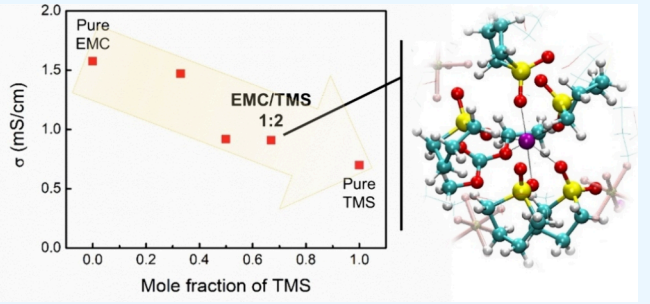

INTRODUCTION

The electrolyte in lithium-ion batteries (LIBs) plays a crucial role in facilitating the transport of lithium ions (Li^+) between the anode and cathode during charge and discharge cycles. The performance and safety of LIBs are inherently linked to the properties of the electrolyte, as it influences key parameters such as energy density, charging speed, and overall battery stability. For optimal performance, electrolytes must exhibit high ionic conductivity, chemical stability, and resistance to electrochemical degradation.[1]

Most commercial LIBs rely on nonaqueous liquid electrolytes, typically composed of lithium hexafluorophosphate ($LiPF_6$) dissolved in organic carbonates like ethylene carbonate (EC), propylene carbonate (PC), dimethyl carbonate (DMC), or ethyl methyl carbonate (EMC).[2,3] These solvents effectively facilitate ion transport, yet they come with significant drawbacks, such as flammability, toxicity, and instability at high voltages and temperatures. Addressing these limitations by developing safer and more stable electrolytes, without compromising on energy density and power output, is essential for advancing LIB technology.

Significant research has focused on conventional solvent systems, particularly those based on EC. However, mixed solvent systems that could overcome the limitations of traditional electrolytes have been relatively underexplored. One promising approach involves combining low-viscosity solvents, such as EMC, with highly stable alternatives such as tetramethylene sulfone (TMS).[4,5] TMS is recognized for its excellent electrochemical stability and oxidation resistance, properties that can enhance electrolyte performance, especially at elevated temperatures. In contrast, EMC, with its lower viscosity, complements TMS by improving ion mobility and reducing the viscosity challenges posed by TMS. Together, these solvents have the potential to create a stable, high-performance electrolyte system.

High oxidation potential of TMS (>6.5 V) and desirable thermal properties, such as a flash point of 166 °C and a boiling point of 285 °C, make it an attractive solvent for high-voltage applications. Despite these advantages, its high viscosity (10.34 cP at 25 °C) and melting point (26 °C) present challenges for practical use by hindering ion movement. To overcome these limitations, researchers have explored blending TMS with lower-viscosity cosolvents. For example, Li et al. proposed a novel electrolyte using lithium bis(oxalato)borate (LiBOB) in a sulfolane/diethyl carbonate

Received: September 27, 2024
Revised: December 25, 2024
Accepted: December 31, 2024
Published: January 7, 2025

(DEC) mixture for high-voltage LIBs,[6] while Watanabe et al. demonstrated improved cycling performance in lithium cells when sulfolane was mixed with ester-based solvents.[7]

Molecular dynamics (MD) simulations have proven invaluable in uncovering the molecular-level interaction within these systems. They provide a detailed examination of solvation structures, ion coordination, and transport mechanisms at the atomic scale.[8,9] Prior studies, including those by Kumar and Seminario and Ong et al.,[10] have utilized MD simulations to explore how solvent environments influence solvation shell structure and ion mobility. These tools provide insights into how EMC and TMS combinations impact the solvation dynamics and overall performance of LIB electrolytes.

Extending this understanding, the solvation structure of Li^+ in organic solvents, particularly in the presence of PF_6^- anions, has been widely examined through both experimental and computational approaches. Research on mixed carbonate electrolytes highlights how solvent composition affects solvation shell rigidity and ion-pairing dynamics.[11] Additionally, PF_6^- anions are known to interact competitively with solvent molecules for coordination sites, influencing solvation environments and ionic mobility. These findings underscore the critical role of solvent-anion interaction in shaping ionic transport properties and emphasize the importance of designing tailored solvent systems to enhance battery performance.[12]

Motivated by these insights, the current study aims to elucidate the effects of TMS on the solvation dynamics and overall performance of Li^+ ions in mixed solvent electrolytes, particularly in combination with EMC. Using MD simulations, we investigate the molecular-level interaction governing Li^+ solvation and transport within $LiPF_6$-based electrolytes containing varying ratios of EMC and TMS. These simulations provide critical insights into how solvent composition influences electrolyte behavior, guiding the development of safer and more efficient electrolyte systems for LIBs.

METHODOLOGY

MD simulations were performed using the GROMACS 2023.2 package to investigate the behavior of lithium-ion electrolytes.[13] The molecular structures of the Li^+ cation, PF_6^- anion, EMC, and TMS are shown in Figure 1. The optimized

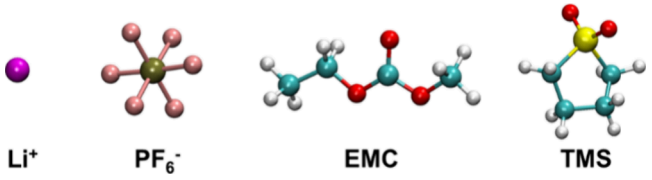

Figure 1. Molecular structures of Li^+, PF_6^-, EMC, and TMS used in MD simulations. The color coding is as follows: purple = lithium, brown = phosphorus, pink = fluorine, cyan = carbon, red = oxygen, white = hydrogen, and yellow = sulfur.

potential for liquid simulations-all atom (OPLS-AA) force field was employed to model the EMC and TMS molecules, ensuring accurate representation of their interaction.[14] The parameters for the Li^+ ions were derived from the work of Lee and Rassiah,[15] while those for the PF_6^- anions were taken from Bhargava and Balasubramanian.[16] Lennard-Jones parameters and partial charges were adopted from the study of Jorgensen and co-workers.[14]

Table 1 summarizes the composition, concentration, and density of the simulation systems. Each system contained 30 $LiPF_6$ molecules and 300 solvent molecules, resulting in a concentration of approximately 1 M. To investigate the effects of different solvent environments, we examined a range of EMC/TMS molar ratios, from pure EMC (1:0) to pure TMS (0:1), as well as intermediate ratios of 2:1, 1:1, and 1:2. These variations were chosen to capture a broad spectrum of solvation dynamics and ionic transport behavior. Periodic boundary conditions were applied in all three dimensions (*XYZ*) to simulate bulk behavior. Long-range electrostatic interaction was calculated using the particle-mesh Ewald (PME) method with a 12 Å cutoff, and Lennard-Jones interaction was treated using the same cutoff distance.

The simulation process began with energy minimization using the steepest descent algorithm, which was employed to eliminate any strained contacts in the system. Following this, the systems were heated to 500 K for 2 ns to ensure sufficient thermal energy, and then cooled from 500 to 300 K over another 2 ns, preventing local configuration confinement and ensuring proper system relaxation. Subsequently, isothermal–isobaric (NPT) equilibration was performed for 2 ns at 300 K and atmospheric pressure, using a 0.001 ps time step, to adjust the system density to the desired level.[17] This was followed by isothermal-isochoric (NVT) equilibration,[18] conducted for 10 ns with the same time step, to further stabilize the temperature and volume of the system. Finally, simulations in the microcanonical ensemble (NVE),[19] were performed for an additional 10 ns with a 0.001 ps time step to compute time-averaged static and dynamic properties of the electrolyte.

RESULTS AND DISCUSSION

Validation of Simulated Densities and Force Field Parameters. The selection of an appropriate force field is essential for obtaining accurate results in MD simulations. Various force fields have been developed, generally falling into two main categories: classical force fields, such as OPLS-AA,[14] and reactive force fields, like ReaxFF.[20] In this study, we employed the OPLS-AA force field, widely recognized for its suitability in simulating electrolytes in MD simulations. The OPLS-AA force field consists of six terms, as represented by the following equation:

$$
\begin{aligned}
U = & \sum_{\text{bonds}} \left[\frac{1}{2}k_{b,i}(r_i - r_{0,i})^2\right] + \sum_{\text{angles}} \left[\frac{1}{2}k_{\theta,i}(\theta_i - \theta_{0,i})^2\right] \\
& + \sum_{\text{improper dihedral}} \left[\frac{C_i}{2}\left(1 + \cos\left(n_i\varphi + \varphi_{0,i}\right)\right)\right] \\
& + \sum_{\text{proper dihedral}} \sum_{n=0}^{5} [C_{n,i}(\cos(180\text{-}\emptyset_i))^n] \\
& + \sum_{i=1}^{N-1} \sum_{j=i+1}^{N} \left[\frac{q_i q_j e^2}{4\pi\varepsilon_0 r_{ij}} + 4\varepsilon_{ij}\left(\left(\frac{\sigma_{ij}}{r_{ij}}\right)^{12} - \left(\frac{\sigma_{ij}}{r_{ij}}\right)^{6}\right)\right]
\end{aligned}
\tag{1}
$$

The simulated densities, along with their associated error bars derived from two independent simulation runs, are provided in Table 1. To validate the accuracy of the OPLS-AA

https://doi.org/10.1021/acsomega.4c08854
ACS Omega 2025, 10, 2141−2149

Table 1. Composition, Concentration, and Density of Systems Containing 30 $LiPF_6$ Molecules and Varying Numbers of EMC and TMS Molecules

		number of molecules					
system	EMC/TMS	$LiPF_6$	EMC	TMS	volume (Å^3)	concentration (M)	simulated density (g/cm^3)
1	1:0 (pure EMC)	30	300	0	37.51 × 37.51 × 37.51	0.94	1.10 ± 0.0006
2	2:1	30	200	100	37.10 × 37.10 × 37.10	1.08	1.19 ± 0.0024
3	1:1	30	100	100	36.64 × 36.64 × 36.64	0.98	1.25 ± 0.0012
4	1:2	30	100	200	36.52 × 36.52 × 36.52	1.01	1.30 ± 0.0023
5	0:1 (pure TMS)	30	0	300	35.88 × 35.88 × 35.88	1.02	1.22 ± 0.0001

force field, we compared the simulated densities of pure EMC and TMS to experimental values,[2,5,21] as shown in Table S1 and Figure S1 in the Supporting Information. The results show excellent agreement, with deviations within 1−3%, confirming the reliability of the force field for pure solvents.

To further validate the performance of the OPLS-AA force field in electrolyte systems, we analyzed Li^+−PF_6^- interaction through radial distribution function (RDF) and coordination number plots for pure EMC and pure TMS (Figures S2 and S3, respectively). The RDF results for pure EMC reveal strong Li^+−PF_6^- ion pairing, with prominent peaks in both Li^+−$P(PF_6^-)$ and Li^+−$F(PF_6^-)$ interactions. In pure TMS, the RDF peaks are less pronounced, indicating reduced ion pairing due to the stronger solvation of Li^+ by TMS molecules. These findings are consistent with previous studies,[22,23] providing confidence in the accuracy of the force field for mixed solvent systems.

While density validates force fields, it cannot fully capture solvation structures or dynamics. RDF and coordination number analyses provide additional reliability for ion-pairing results. Although direct experimental data are unavailable, future work could compare solvation free energies from quantum mechanical or QM/MM methods. Polarizable force fields could further enhance validation and improve MD simulation accuracy for electrolytes.

Solvation Structure. Figure 2 shows the Li^+ solvation structure in pure EMC and pure TMS systems, highlighting

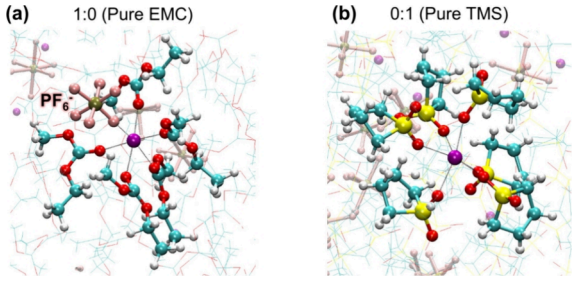

Figure 2. Structural snapshots of Li^+ solvation environments in (a) pure EMC and (b) pure TMS. The black dashed lines indicate the coordination between Li^+ and surrounding solvent molecules.

their distinct solvation environments. In pure EMC (Figure 2a), Li^+ forms a loosely structured solvation shell coordinated by EMC molecules, while the PF_6^- anion is positioned near Li^+ and contributes to the solvation structure. This configuration suggests partial interaction between Li^+ and PF_6^- in the EMC system. In contrast, in pure TMS (Figure 2b), the solvation shell is more structured, with six TMS molecules tightly coordinating around Li^+. The PF_6^- anion is displaced to the outer shell, indicating a separation between Li^+ and PF_6^-.

Figure 3 shows the solvation structure of Li^+ in mixed EMC/TMS systems with different molar ratios. In the 2:1 EMC/TMS system (Figure 3a), Li^+ is coordinated by two EMC molecules and three TMS molecules, while PF_6^- remains close to Li^+, indicating partial ion pairing similar to that in pure EMC. In the 1:1 EMC/TMS system (Figure 3b), both EMC and TMS molecules participate in the solvation shell, and PF_6^- is located near Li^+. In the 1:2 EMC/TMS system (Figure 3c), TMS dominates the solvation shell, and PF_6^- is fully excluded from the immediate vicinity of Li^+, indicating a greater separation between Li^+ and PF_6^-.

These findings reveal that increasing TMS content enhances the separation between Li^+ and PF_6^- by allowing TMS to dominate the solvation shell. This result aligns with previous studies showing that higher TMS concentrations lead to greater Li^+ and PF_6^- separation.[9,23,24] By reducing the likelihood of ion pair formation, this separation could improve ionic conductivity in the electrolyte.

To gain insights into the solvation structure and coordination environment of Li^+ ions in mixed EMC/TMS solvent systems, we performed RDF and coordination number analysis based on MD simulation trajectories. The RDF, denoted as $g(r)$, represents the probability of finding a particle at a distance r from a reference particle, providing the local structure of ions and solvent molecules. This analysis helps quantify the spatial arrangement and interaction among the different components of the electrolyte mixture. The RDF for a pair of particles x and y is mathematically defined as[25]

$$g(r) = \frac{n(r)}{4\pi r^2 \rho dr} \tag{2}$$

where $n(r)$ is the number of y atoms at a radial distance r from a reference particle x, $4\pi r^2 dr$ is the volume of a shell of thickness dr at r, and ρ is the bulk number density of y atoms.

The number of atoms within a sphere of radius r surrounding a reference ion is determined by integrating the RDF, which yields the coordination number, $N(r)$, calculated as[26]

$$N(r) = 4\pi\rho \int_0^r r^2 g(r) dr \tag{3}$$

Figure 4 provides insights into the interaction of Li^+ and PF_6^- with solvent molecules (EMC and TMS) across varying EMC/TMS compositions through the RDF and coordination number.

In Figure 4a, the RDF peak for Li^+−O_c(EMC) appears strongly at ∼2.3 Å in pure EMC, indicating close coordination between Li^+ and carbonyl oxygen atoms. As the TMS content increases, the intensity of this peak decreases, reflecting the displacement of EMC molecules from the first solvation shell of Li^+. The peak heights drop from 14.5 (pure EMC) to 8.7 (2:1 EMC/TMS), 7.0 (1:1 EMC/TMS), and 4.0 (1:2 EMC/

https://doi.org/10.1021/acsomega.4c08854
ACS Omega 2025, 10, 2141−2149

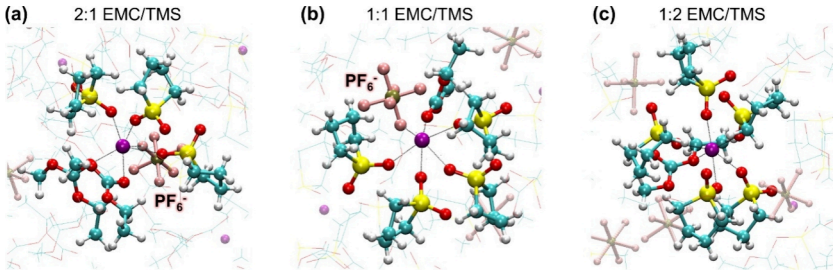

Figure 3. Structural snapshots of Li^+ solvation environments in different EMC/TMS molar ratios: (a) $Li(EMC)_2(TMS)_3PF_6$ (EMC/TMS = 2:1), (b) $Li(EMC)_1(TMS)_4PF_6$ (EMC/TMS = 1:1), and (c) $[Li(EMC)_1(TMS)_5]^+$ (EMC/TMS = 1:2). The black dashed lines indicate the coordination between Li^+ and surrounding solvent molecules.

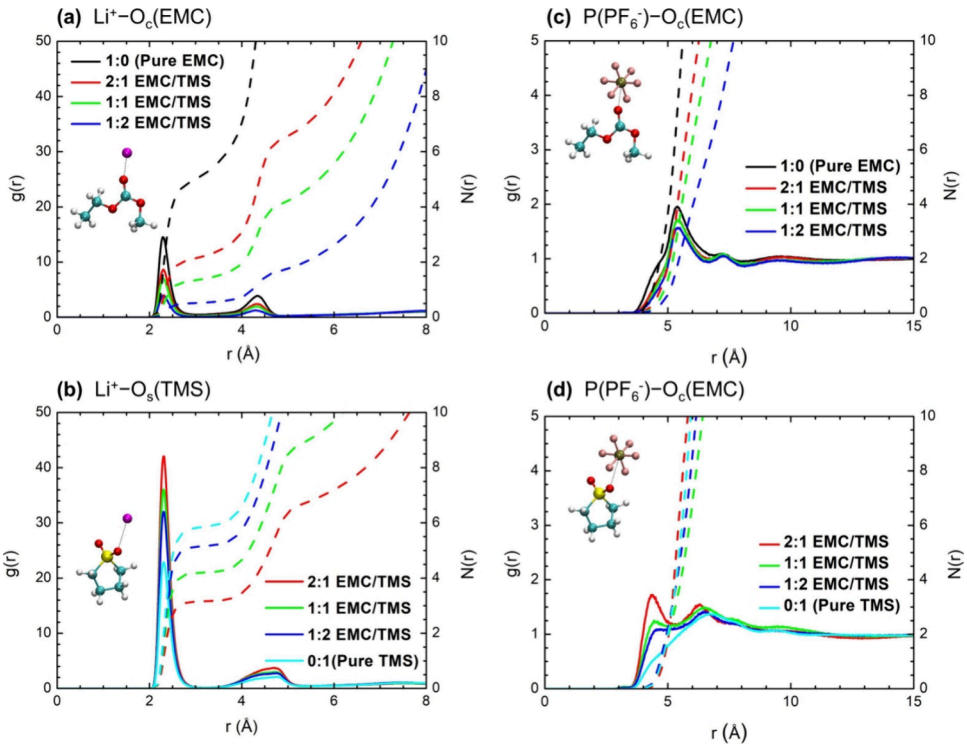

Figure 4. Radial distribution function $g(r)$ (solid lines) and coordination number $N(r)$ (dashed lines) for interaction involving Li^+ and PF_6^- with solvent molecules: (a) $Li^+–O_c$(EMC), (b) $Li^+–O_s$(TMS), (c) $P(PF_6^-)–O_c$(EMC), and (d) $P(PF_6^-)–O_s$(TMS). Data are shown for systems with varying EMC/TMS ratios: 1:0 (pure EMC), 2:1, 1:1, 1:2, and 0:1 (pure TMS).

TMS). Similarly, the coordination number for O_c(EMC) declines from 5.1 (pure EMC) to 2.2 (2:1 EMC/TMS), 1.4 (1:1 EMC/TMS), and 0.6 (1:2 EMC/TMS). These trends show that the number of EMC molecules around Li^+ decreases as TMS concentration increases.

Figure 4b shows the RDF for $Li^+–O_s$(TMS), where the coordination number increases as TMS content rises, indicating the growing dominance of TMS in the Li^+ solvation shell. However, the RDF peak height decreases with higher TMS concentrations, reflecting reduced localization and dynamic competition among TMS molecules in the solvation shell. The coordination number for O_s(TMS) decreases as TMS content is reduced, moving from 5.9 (pure TMS) to 5.2 (1:2 EMC/TMS), 4.2 (1:1 EMC/TMS), and 3.2 (2:1 EMC/TMS), confirming that TMS displaces EMC in the solvation shell of Li^+ as its concentration increases. The plateaus in the coordination number integrals (dashed lines) across all panels reinforce these findings. TMS demonstrates stronger interaction with Li^+ compared to EMC, effectively displacing EMC molecules from the first solvation shell as its concentration increases. In addition, PF_6^- becomes excluded from the immediate environment of Li^+, supporting the conclusion that TMS-rich systems reduce ion pairing.

Figure 4c,d examine the proximity of PF_6^- to EMC and TMS oxygen atoms, respectively. In Figure 4c, the RDF peak between $P(PF_6^-)$ and O_c(EMC) is weak across all solvent compositions, indicating limited interaction. As TMS concentration increases, the RDF peak intensity decreases further, indicating the diminished presence of EMC in the ionic environment and reduced PF_6^-–EMC proximity in TMS-rich systems.

Figure 4d shows the proximity of PF_6^- to the sulfonyl oxygen atoms (O_s) of TMS. Interestingly, the RDF peak in pure TMS systems (0:1) is lower than in mixed systems, suggesting reduced PF_6^- proximity to TMS oxygen atoms in TMS-dominant environments. This behavior can be attributed to the strong coordination of TMS with Li^+, which creates a tightly structured solvation shell. The tight Li^+–TMS solvation

https://doi.org/10.1021/acsomega.4c08854
ACS Omega 2025, 10, 2141−2149

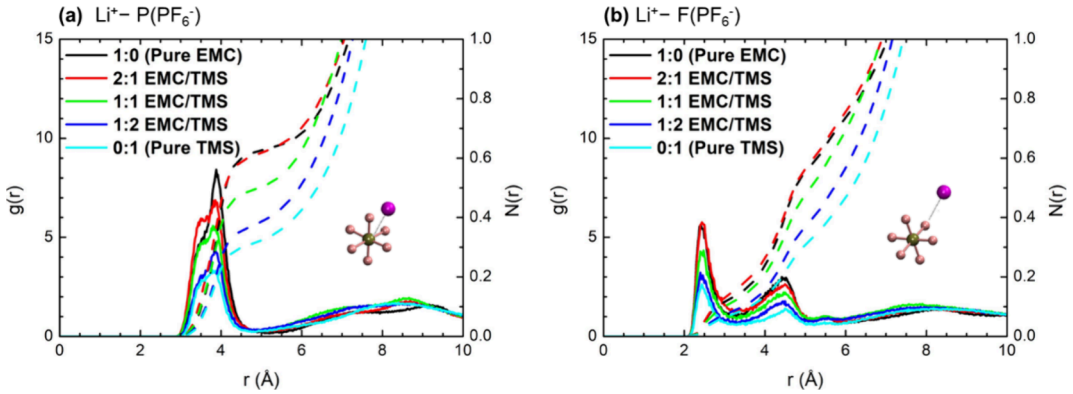

Figure 5. Radial distribution function $g(r)$ (solid lines) and coordination number $N(r)$ (dashed lines) for interaction between (a) Li^+−$P(PF_6^-)$ and (b) Li^+−$F(PF_6^-)$. Data are shown for systems with varying EMC/TMS ratios: 1:0 (pure EMC), 2:1, 1:1, 1:2, and 0:1 (pure TMS).

shell reduces the availability of TMS oxygen atoms for PF_6^- proximity and displaces PF_6^- further from the immediate ionic environment, weakening PF_6^- interaction with TMS.

Figure 5 provides the RDF and coordination number for the interaction between Li^+ and the phosphorus (P) and fluorine (F) atoms of PF_6^- in systems with varying EMC/TMS ratios. These results offer insights into the extent of ion pairing between Li^+ and PF_6^- under different solvent compositions.

In Figure 5a, the RDF for Li^+−$P(PF_6^-)$ shows a prominent peak at ∼3.8 Å, indicating a coordination interaction between Li^+ and the phosphorus atom of PF_6^-. The peak heights decrease as the TMS content increases, from 8.4 in the pure EMC system (1:0 EMC/TMS) to 6.9 (2:1 EMC/TMS), 5.6 (1:1 EMC/TMS), 4.4 (1:2 EMC/TMS), and 3.3 in the pure TMS system (0:1 EMC/TMS). This trend reflects a reduction in the interaction strength between Li^+ and PF_6^- as TMS concentration increases. The sharper RDF peak in pure EMC indicates stronger and more stable ion pairing in EMC-rich systems. In contrast, the lower and broader peaks in TMS-rich systems suggest weaker interaction and greater separation between Li^+ and PF_6^-. The coordination number for Li^+−$P(PF_6^-)$, shown by the dashed lines, further confirms these observations. In pure EMC, the coordination number is approximately 0.6, meaning that, on average, each Li^+ ion is coordinated by 0.6 phosphorus atoms of PF_6^-. As TMS content increases, the coordination number decreases, dropping to ∼0.2 in the pure TMS system. This indicates that TMS effectively displaces PF_6^- anions from the immediate solvation shell of Li^+, reducing ion pairing.

Figure 5b shows the RDF for Li^+−$F(PF_6^-)$, with a primary peak at ∼3.6 Å and a smaller secondary peak at ∼4.5 Å. The primary peak represents the direct coordination between Li^+ and the fluorine atoms of PF_6^- that are closest to Li^+ in the solvation shell. The secondary peak corresponds to interaction with fluorine atoms positioned farther away within the tetrahedral structure of PF_6^-. As TMS content increases, both peaks decrease in intensity, indicating weaker ion pairing. The coordination number for Li^+−$F(PF_6^-)$ also decreases with higher TMS content, confirming that TMS displaces PF_6^- from the Li^+ solvation shell, promoting ion dissociation and a more separated ion environment.

This further supports the conclusion that higher TMS content weakens the interaction between Li^+ and PF_6^-. The reduced interaction between Li^+ and PF_6^- in TMS-rich systems contributes to a more dissociated ion environment, as also reflected by the structural snapshots in Figure 3, which show greater separation between Li^+ and PF_6^- as TMS concentration increases.

However, while the displacement of PF_6^- from the Li^+ solvation shell reduces ion pairing and contributes to a more dissociated ion environment, the higher affinity of TMS for Li^+ simultaneously tightens the solvation shell around Li^+. This increased rigidity hinders Li^+ mobility by increasing its effective mass. These dual effects result in a trade-off between the benefits of reduced ion pairing and the drawbacks of a more rigid solvation shell, particularly at intermediate TMS concentrations (e.g., EMC/TMS = 1:1). As a result, Li^+ mobility is lowest at intermediate TMS concentrations, where these opposing effects are most pronounced. Beyond this point, the solvation shell stabilizes, allowing for slight improvements in mobility at higher TMS concentrations.

Dynamical Properties. Transport properties of electrolytes play a critical role in assessing battery performance. Faster movement of Li^+ ions within the solution leads to higher current density in LIBs. By examining ion trajectories under zero electric field conditions during MD simulations, we can determine the diffusion coefficient of ions and the ionic conductivity of the solution.[27]

In our study, ion transport in MD simulations was quantified using the diffusion coefficient (D), which was computed through least-squares fitting of the mean-squared displacement (MSD) data.[28] This fitting process can be expressed using the following equation:

$$D = \lim_{\Delta t \to \infty} \frac{<\mathrm{MSD}_i(t)>}{6t} \tag{4}$$

In the eq 4, $\mathrm{MSD}_i(t)$ represents the mean-squared displacement of the center of mass of a component i after time t, < > denotes an ensemble average. The diffusion coefficient were calculated using the MSD curves within the linear region corresponding to the time interval of 1−9 ns. This interval was selected to ensure reliable fitting by excluding the 0−1 ns region (to avoid distortions from the ballistic motion phase) and the 9−10 ns range (to minimize statistical fluctuations and finite-size effects). For Li^+ ions, the MSD quantifies the motion of individual atoms, whereas for PF_6^- ions, the MSD captures the dynamics of the molecular center of mass. By separately accounting for atomic and molecular motions, this approach ensures precise estimates of the ionic diffusion coefficient.

To ensure the reliability of the calculated D values and address equilibration concern, the MSD data were further

https://doi.org/10.1021/acsomega.4c08854
ACS Omega 2025, 10, 2141−2149

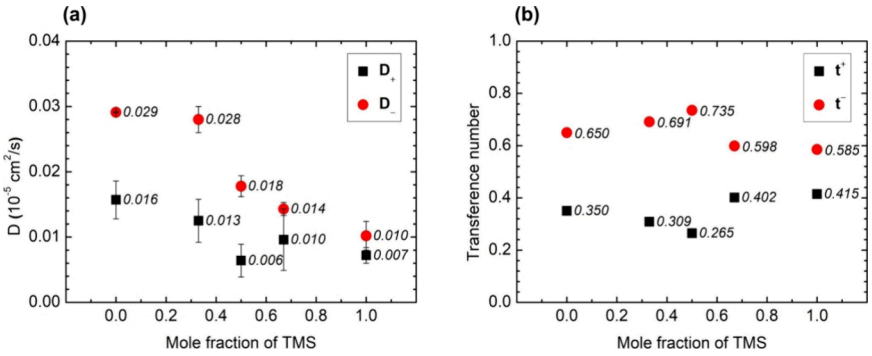

Figure 6. (a) Diffusion coefficient of Li^+(D_+) ions and PF_6^-anions ($D\_$) and (b) transference number of Li^+(t^+) ions and PF_6^-anions (t^-) on increasing the mole fraction of TMS.

analyzed across overlapping trajectory subsets (1−5, 5−9, and 1−9 ns). This addition analysis verifies that the D values has reached a steady state and is independent of the specific trajectory segment. As illustrated in Figure S7, the MSD plots for all systems with varying EMC/TMS ratios (1:0, 2:1, 1:1, 1:2, and 0:1) demonstrated a clear linear relationship with time over the investigated time intervals. The D values calculated from these subsets, presented in Table S2, shows consistent values, confirming that the dynamic properties are representative of an equilibrated system. These findings align with established practices in MD simulations for assessing steady-state behavior.[29]

Building on this analysis, the transference number emerges as another critical parameter, offering insights into the relative mobility of active Li^+ ions compared to the migration of both cations and anions.[30] In nonaqueous solutions, the Li^+ transference number typically falls within the range of 0.20 to 0.40, depending on the properties of the solvents and salts.[31] For a 1:1 electrolyte, donated as MX, consisting of a cation M^+ and anion X^-, the transference number can be estimated by considering the diffusion coefficient of both the cation and anion, as shown in the following equation:

$$t^+ = \frac{D_+}{D_+ + D\_}, \; t^- = \frac{D\_}{D_+ + D\_} \tag{5}$$

The ionic conductivity (σ) for the system can be calculated using the Nernst−Einstein equation,[28,32] which is expressed as follows:

$$\sigma = \frac{N_{pair} e^2}{V k_B T}(q_+^2 D_+ + q\_^2 D\_) \tag{6}$$

where N_{pair} is the number of ion pairs, e is electric charge, q_+ and $q\_$ are the total charges on cation and anion, respectively, D_+ and $D\_$ are the diffusion coefficient of cation and anion, respectively, V is the simulation box volume, T is the temperature, and k_B is the Boltzmann constant. The Nernst−Einstein equation, commonly applied to dilute solutions, was used in this study as a reference framework to estimate ionic conductivity trends in the mixed electrolyte systems. While this equation assumes uncorrelated ion motion and does not account for the strong ion−ion correlations and ion pairing present in concentrated solutions, it provides valuable qualitative insights into how solvent composition influences ionic transport properties. These trends are consistent with structural data obtained from RDF and coordination number analyses. Future work will incorporate advanced techniques, such as Onsager transport theory,[33] to address ion correlation effects and improve the quantitative accuracy of conductivity predictions in concentrated electrolyte systems.

Figure 6a illustrates the diffusion coefficient (D) of Li^+ and PF_6^- ions. The D values of Li^+ ions decrease from 0.0157×10^{-5} cm^2/s in pure EMC (1:0) to 0.0072×10^{-5} cm^2/s in pure TMS (0:1). Similarly, D values for PF_6^- ions decrease from 0.0291×10^{-5} cm^2/s (1:0) to 0.0102×10^{-5} cm^2/s (0:1). The lower mobility of Li^+ compared to PF_6^- is due to its stable and extensive solvation shell, which increases its effective mass and restricts diffusion. Li^+ forms strong interaction with solvent molecules, particularly TMS, creating a tightly bound solvation environment. In contrast, PF_6^-, being larger and less charge-dense, experiences weaker solvation effects and diffuses more freely. The addition of TMS also increases the viscosity of the medium, further reducing the diffusion coefficients of both ions. These trends reflect the interplay between solvation dynamics, ion size, and solvent composition in influencing ionic mobility.

The transference number (t^+ for Li^+ and t^- for PF_6^-) as a function of the mole fraction of TMS, shown in Figure 6b, also reflects these dynamics. Across all systems, the transference number of Li^+ is less than 0.5, indicating that PF_6^- anions contribute more to the total ionic conductivity. This dominance of anions in charge transport is attributed to the tightly packed solvation shell around Li^+, which increases its effective mass and reduces its mobility. As TMS is added to the mixture, the solvation shell around Li^+ becomes stronger due to the higher affinity of TMS for Li^+, further limiting its movement.

Interestingly, the simulation results reveal a decreasing trend in Li^+ transference number as the mole fraction of TMS increases up to 0.50 (EMC/TMS = 1:1), where the lowest transference number value is observed. This trend is likely due to the strong interaction between Li^+ and TMS, which restricts Li^+ mobility. While the changes in Li^+ transference number are small, they are supported by the error bars for the underlying diffusion coefficient shown in Figure 6a, which indirectly validates the calculated transference number. Furthermore, structural data, including RDF and coordination number analyses, corroborate these trends by demonstrating changes in solvation dynamics and ion-pairing behavior with increasing TMS concentration. Together, these findings confirm the robustness of the observed trends despite the minimal differences.

At higher TMS concentrations (TMS mole fraction > 0.50), the Li^+ transference number begins to increase slightly,

https://doi.org/10.1021/acsomega.4c08854
ACS Omega 2025, 10, 2141−2149

suggesting that the solvation environment around Li^+ may stabilize, allowing for slightly improved Li^+ mobility compared to intermediate TMS concentrations. While PF_6^- anions dominate the charge transport in all systems, the variation in Li^+ transference number with increasing TMS mole fraction highlights the complex relationship between solvent composition, solvation structure, and ion mobility. Optimizing the EMC/TMS ratio is crucial for enhancing the overall performance of the electrolyte, particularly by balancing the contributions of Li^+ and PF_6^- to the ionic conductivity.

Regarding the overestimated Li^+ transference number reported in some literature, these differences may arise from the inherent assumptions made in experimental methodology, such as neglecting ion−ion correlations and solvent dynamics that influence ion transport properties. Our simulations explicitly incorporate these factors, capturing the detailed solvation dynamics, ion-pairing, and their impact on Li^+ mobility. The trends in Li^+ transference number observed across varying TMS mole fractions are consistent with the solvation structure and ion dynamics revealed by our Coulombic interaction analysis, supporting the robustness and reliability of our computational approach.

The ionic conductivity (σ) of the electrolyte solutions with varying molar ratios of EMC and TMS is shown in Figure 7.

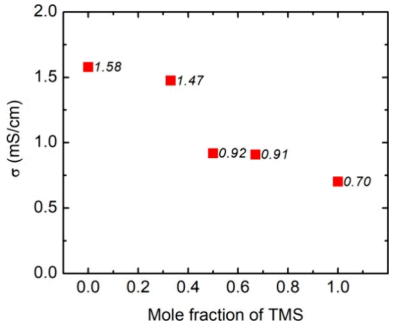

Figure 7. Ionic conductivity (σ) of the electrolyte solutions on increasing the mole fraction of TMS.

The highest ionic conductivity (1.58 mS/cm) was observed in the pure EMC system (EMC/TMS = 1:0), which aligns with an earlier MD study by Saitoh et al.[34] However, experimental measurements of the conductivity of the solution for 1 M $LiPF_6$ in EMC at 298 K showed higher values (∼4 mS/cm). The lowest ionic conductivity (0.7 mS/cm) was observed in the pure TMS system (EMC/TMS = 0:1), which is attributed to the high viscosity of TMS (10.34 cP at 298 K). As TMS molecules are added to the mixture, the ionic conductivity decreases, consistent with the results reported by Kumar et al.[9] Interestingly, the ionic conductivity remains relatively stable as the mole fraction of TMS increases from 0.50 (EMC/TMS = 1:1) to 0.67 (EMC/TMS = 2:1), with values of 1.47 and 0.92 mS/cm, respectively, reflecting the balance between solvation dynamics and solvent composition.

To understand these trends, the short-range Coulombic (Coul-SR) interaction, shown in Figure S8, provides insights into the solvation dynamics influencing ionic transport. The interaction energy between Li^+ and TMS is significantly stronger and more negative compared to Li^+-EMC, indicating a more rigid solvation shell in TMS-rich systems. This rigidity restricts the mobility of Li^+, reducing its contribution to ionic conductivity. Additionally, Li^+−PF_6^- interaction remains strong across the trajectory, signifying persistent ion-pairing that limits the availability of free ions for charge transport. The interplay between solvation shell rigidity and ion pairing contributes to the observed decrease in conductivity as the TMS content increases. These findings align with the diffusion coefficient and transference number trends shown in Figure 6a,b, highlighting the impact of solvation structure and solvent composition on ionic mobility.

Despite these qualitative consistency, a notable gap remains between simulated and experimental conductivity values. This discrepancy stems from limitations in the nonpolarizable OPLS-AA force field used in this study. By underestimating dielectric screening and overestimating ion-pairing tendency, the force field results in a more rigid solvation environment and reduced Li^+ mobility. Consequently, the simulated ionic conductivity values are lower than experimental observations, where polarization effects enhance Li^+ mobility and reduce ion-pairing. These findings underscore the importance of accurately capturing dielectric and polarization effects in future simulations to bridge this gap. Incorporating advanced simulation approaches, such as polarizable force fields or machine-learned potentials,[35] could provide a more realistic representation of ion dynamics and conductivity. These improvements would help reduce discrepancy between simulated and experimental results, enabling more accurate predictions of electrolyte performance and guiding the design of advanced solvent systems.

Taken together, the trends in ionic conductivity and transference numbers highlight the relationship between solvent composition, solvation structure, and ion mobility. The Coul-SR analysis further supports these findings, demonstrating the role of Li^+-TMS interaction in shaping solvation rigidity and ionic transport. These insights emphasize the importance of balancing EMC and TMS ratios to optimize electrolyte performance and achieve the desired transport properties.

CONCLUSIONS

This study examined the potential of mixed solvent systems, specifically ethyl methyl carbonate (EMC) and tetramethylene sulfone (TMS), to modify ion solvation and ionic conductivity in LIB electrolytes using molecular dynamics simulations. The findings revealed that increasing the TMS content significantly altered the solvation environment. TMS strongly coordinated with Li^+, displacing PF_6^- anions from the solvation shell and promoting greater separation between Li^+ and PF_6^-, which reduced ion pairing and enhanced ionic conductivity. A 1:2 EMC/TMS ratio was found to offer the optimal combination of properties, yielding an ionic conductivity of 0.91 mS/cm and a Li^+ transference number of 0.40. However, as the TMS content increased further, the solvation shell tightened around Li^+, limiting its mobility and reducing the overall ionic conductivity. These results emphasize the importance of balancing EMC and TMS ratios to optimize electrolyte performance. This study underscores the molecular interaction that governs electrolyte behavior, offering valuable insights for the design of safer and more efficient electrolytes for LIBs. Nonetheless, the study also underscores the limitations of the nonpolarizable OPLS-AA force field, which underestimates dielectric screening and overestimates ion-pairing tendency. Addressing these limitations in future work by incorporating polarizable force fields or machine-learned potentials could improve the representation of dielectric effects and ion−

https://doi.org/10.1021/acsomega.4c08854
ACS Omega 2025, 10, 2141−2149

solvent dynamics, enhancing the predictive power of MD simulations. In summary, this study elucidates the impact of EMC/TMS ratios on solvation dynamics and ionic conductivity, offering a solid foundation for future research aimed at developing advanced electrolytes for next-generation LIBs.

■ ASSOCIATED CONTENT

Supporting Information

The Supporting Information is available free of charge at https://pubs.acs.org/doi/10.1021/acsomega.4c08854.

Supporting Information details density validation (Table S1, Figure S1), solvation and coordination structures of Li^+-PF_6^- pairs in EMC/TMS systems (Figures S2−S4, S6), energy and temperature stability in 1:1 EMC/TMS mixture (Figure S5), ion transport dynamics (Figure S7), diffusion coefficients (Table S2), and Coulombic interactions between Li^+ and its coordinating species (Figure S8) (PDF)

■ AUTHOR INFORMATION

Corresponding Author

Manaswee Suttipong − *Department of Chemical Technology, Faculty of Science, Chulalongkorn University, Bangkok 10330, Thailand;* orcid.org/0009-0000-8702-2365; Email: manaswee.s@chula.ac.th

Authors

Jitti Kasemchainan − *Department of Chemical Technology, Faculty of Science, Chulalongkorn University, Bangkok 10330, Thailand;* orcid.org/0000-0002-5341-1650

Siriporn Teeraburanapong − *Department of Chemical Technology, Faculty of Science, Chulalongkorn University, Bangkok 10330, Thailand*

Complete contact information is available at: https://pubs.acs.org/10.1021/acsomega.4c08854

Notes

The authors declare no competing financial interest.

■ ACKNOWLEDGMENTS

This research was supported by the Ratchadapiseksompotch Fund, Chulalongkorn University, the Thailand Science Research and Innovation Fund, Chulalongkorn University, and the Program Management Unit for Human Resources & Industrial Development, Research & Innovation (B41G670026). The authors sincerely thank Pongpon Pipattanachaiyanan for his valuable contribution in performing supplementary calculations, which were crucial for addressing reviewer comments and strengthening this study.

■ REFERENCES

(1) (a) Cheng, H.; Ma, Z.; Kumar, P.; Liang, H.; Cao, Z.; Xie, H.; Cavallo, L.; Kim, H.; Li, Q.; Sun, Y.-K.; et al. High Voltage Electrolyte Design Mediated by Advanced Solvation Chemistry Toward High Energy Density and Fast Charging Lithium-Ion Batteries. *Adv. Energy Mater.* **2024**, *14* (18), No. 2304321. (b) Franco, A. A.; Rucci, A.; Brandell, D.; Frayret, C.; Gaberscek, M.; Jankowski, P.; Johansson, P. Boosting Rechargeable Batteries R&D by Multiscale Modeling: Myth or Reality? *Chem. Rev.* **2019**, *119* (7), 4569−4627. Review. (c) Li, M.; Wang, C.; Chen, Z.; Xu, K.; Lu, J. New Concepts in Electrolytes. *Chem. Rev.* **2020**, *120* (14), 6783−6819. (d) Petibon, R.; Xia, J.; Ma, L.; Bauer, M. K. G.; Nelson, K. J.; Dahn, J. R. Electrolyte System for High Voltage Li-Ion Cells. *J. Electrochem. Soc.* **2016**, *163* (13), A2571.

(2) (a) Wang, A. A.; Hou, T.; Karanjavala, M.; Monroe, C. W. Shifting-reference concentration cells to refine composition-dependent transport characterization of binary lithium-ion electrolytes. *Electrochim. Acta* **2020**, *358*, No. 136688. (b) Wang, A. A.; Persa, D.; Helin, S.; Smith, K. P.; Raymond, J. L.; Monroe, C. W. Compressibility of Lithium Hexafluorophosphate Solutions in Two Carbonate Solvents. *Journal of Chemical & Engineering Data* **2023**, *68* (4), 805−812.

(3) Eisele, L.; Laszczynski, N.; Görg, M.; Schneider, M.; Burger, S.; Radkte, V.; Lucht, B.; Krossing, I. Investigation of Mixtures of BF3 Carbonates and LiX (X = OCH2CF3, OC(H)(CF3)2, CO2CF3) as Novel Electrolyte Systems for Lithium Ion Batteries. *J. Electrochem. Soc.* **2020**, *167* (8), No. 080507.

(4) (a) Dokko, K.; Watanabe, D.; Ugata, Y.; Thomas, M. L.; Tsuzuki, S.; Shinoda, W.; Hashimoto, K.; Ueno, K.; Umebayashi, Y.; Watanabe, M. Direct Evidence for Li Ion Hopping Conduction in Highly Concentrated Sulfolane-Based Liquid Electrolytes. *J. Phys. Chem. B* **2018**, *122* (47), 10736−10745. (b) Jia, H.; Xu, Y.; Zou, L.; Gao, P.; Zhang, X.; Taing, B.; Matthews, B. E.; Engelhard, M. H.; Burton, S. D.; Han, K. S.; et al. Sulfone-based electrolytes for high energy density lithium-ion batteries. *J. Power Sources* **2022**, *527*, No. 231171. (c) Okamoto, Y.; Tsuzuki, S.; Tatara, R.; Ueno, K.; Dokko, K.; Watanabe, M. High Transference Number of Na Ion in Liquid-State Sulfolane Solvates of Sodium Bis(fluorosulfonyl)amide. *J. Phys. Chem. C* **2020**, *124* (8), 4459−4469. (d) Wu, W.; Bai, Y.; Wang, X.; Wu, C. Sulfone-based high-voltage electrolytes for high energy density rechargeable lithium batteries: Progress and perspective. *Chin. Chem. Lett.* **2021**, *32* (4), 1309−1315.

(5) Tilstam, U. Sulfolane: A Versatile Dipolar Aprotic Solvent. *Org. Process Res. Dev.* **2012**, *16* (7), 1273−1278.

(6) Li, S.; Zhao, Y.; Shi, X.; Li, B.; Xu, X.; Zhao, W.; Cui, X. Effect of sulfolane on the performance of lithium bis(oxalato)borate-based electrolytes for advanced lithium ion batteries. *Electrochim. Acta* **2012**, *65*, 221−227.

(7) Watanabe, Y.; Kinoshita, S. i.; Wada, S.; Hoshino, K.; Morimoto, H.; Tobishima, S. I. Electrochemical properties and lithium ion solvation behavior of sulfone-ester mixed electrolytes for high-voltage rechargeable lithium cells. *J. Power Sources* **2008**, *179* (2), 770−779.

(8) (a) Núñez-Rojas, E.; González, I.; Guzmán-González, G.; Alejandre, J. Molecular dynamics simulations for liquid electrolytes of propylene carbonate with LiTFSI, LiPF6, and LiBF4 salts. *J. Mol. Liq.* **2023**, *390*, No. 122983. (b) Parida, R.; Pahari, S.; Jana, M. Introducing the potency of new boron-based heterocyclic anion receptor additives to regulate the solvation and transport properties of Li-ions in ethylene carbonate electrolyte of Li-Ion battery: An atomistic molecular dynamics study. *J. Power Sources* **2022**, *521*, No. 230962. (c) Ravikumar, B.; Mynam, M.; Rai, B. Effect of Salt Concentration on Properties of Lithium Ion Battery Electrolytes: A Molecular Dynamics Study. *J. Phys. Chem. C* **2018**, *122* (15), 8173−8181. (d) Ravikumar, B.; Mynam, M.; Repaka, S.; Rai, B. Solvation shell dynamics explains charge transport characteristics of LIB electrolytes. *J. Mol. Liq.* **2021**, *338*, No. 116613. (e) Seo, J.; Choi, S.; Singh, R.; Choi, J.-H. Spatial inhomogeneity and molecular aggregation behavior in aqueous binary liquid mixtures. *J. Mol. Liq.* **2023**, *369*, No. 120949. 10.1039/D2CP06020E. (f) Zaboli, A.; Raissi, H.; Hashemzadeh, H.; Farzad, F. Toward efficient electrodes for a high-performance fast-charge Li-ion battery: molecular dynamics simulation and DFT calculations. *Phys. Chem. Chem. Phys.* **2023**, *25* (35), 23937−23953. (g) Molashahi, M.; Modarress, H.; Nasernejad, B.; Amjad-Iranagh, S.; Ghalami Choobar, B. Structural and Transport Properties of Novel High-Transference Number Electrolytes Based on Perfluoropolyether-block-Poly(ethylene oxide) for Application in Lithium-Ion Batteries: A Molecular Dynamics Simulation Study. *Macromolecules* **2022**, *55* (23), 10556−10575. (h) Van der Ven, A.; Deng, Z.; Banerjee, S.; Ong, S. P. Rechargeable Alkali-Ion Battery Materials: Theory and Computation. *Chem. Rev.* **2020**, *120* (14), 6977−7019. (i) Yao, N.; Chen, X.; Fu, Z.-H.; Zhang, Q. Applying Classical, Ab Initio, and Machine-Learning Molecular Dynamics

Simulations to the Liquid Electrolyte for Rechargeable Batteries. *Chem. Rev.* **2022**, *122* (12), 10970−11021.
(9) Kumar, G.; Kartha, T. R.; Mallik, B. S. Novelty of Lithium Salt Solution in Sulfone and Dimethyl Carbonate-Based Electrolytes for Lithium-Ion Batteries: A Classical Molecular Dynamics Simulation Study of Optimal Ion Diffusion. *J. Phys. Chem. C* **2018**, *122* (46), 26315−26325.
(10) (a) Ong, M. T.; Verners, O.; Draeger, E. W.; van Duin, A. C. T.; Lordi, V.; Pask, J. E. Lithium Ion Solvation and Diffusion in Bulk Organic Electrolytes from First-Principles and Classical Reactive Molecular Dynamics. *J. Phys. Chem. B* **2015**, *119* (4), 1535−1545. (b) Kumar, N.; Seminario, J. M. Lithium-Ion Model Behavior in an Ethylene Carbonate Electrolyte Using Molecular Dynamics. *J. Phys. Chem. C* **2016**, *120* (30), 16322−16332.
(11) Shim, Y. Computer simulation study of the solvation of lithium ions in ternary mixed carbonate electrolytes: free energetics, dynamics, and ion transport. *Phys. Chem. Chem. Phys.* **2018**, *20* (45), 28649−28657. 10.1039/C8CP05190A.
(12) Chang, T.-M.; Dang, L. X. Li+ solvation and kinetics of Li+−BF4−/PF6−ion pairs in ethylene carbonate. A molecular dynamics study with classical rate theories. *J. Chem. Phys.* **2017**, *147* (16), 161709. (acccessed 11/21/2024).
(13) Abraham, M. J.; Murtola, T.; Schulz, R.; Páll, S.; Smith, J. C.; Hess, B.; Lindahl, E. GROMACS: High performance molecular simulations through multi-level parallelism from laptops to supercomputers. *SoftwareX* **2015**, *1−2*, 19−25.
(14) (a) Jorgensen, W. L.; Maxwell, D. S.; Tirado-Rives, J. Development and Testing of the OPLS All-Atom Force Field on Conformational Energetics and Properties of Organic Liquids. *J. Am. Chem. Soc.* **1996**, *118* (45), 11225−11236. (b) Jorgensen, W. L.; Tirado-Rives, J. The OPLS [optimized potentials for liquid simulations] potential functions for proteins, energy minimizations for crystals of cyclic peptides and crambin. *J. Am. Chem. Soc.* **1988**, *110* (6), 1657−1666.
(15) Lee, S. H.; Rasaiah, J. C. Molecular Dynamics Simulation of Ion Mobility. 2. Alkali Metal and Halide Ions Using the SPC/E Model for Water at 25 °C. *J. Phys. Chem.* **1996**, *100* (4), 1420−1425.
(16) Bhargava, B. L.; Balasubramanian, S. Refined potential model for atomistic simulations of ionic liquid [bmim][PF6]. *J. Chem. Phys.* **2007**, *127* (11), 114510. (acccessed 9/27/2024).
(17) Berendsen, H. J. C.; Postma, J. P. M.; van Gunsteren, W. F.; DiNola, A.; Haak, J. R. Molecular dynamics with coupling to an external bath. *J. Chem. Phys.* **1984**, *81* (8), 3684−3690. (acccessed 9/27/2024).
(18) Bussi, G.; Donadio, D.; Parrinello, M. Canonical sampling through velocity rescaling. *J. Chem. Phys.* **2007**, *126* (1), No. 014101. (acccessed 9/27/2024).
(19) Griffiths, R. B. Microcanonical Ensemble in Quantum Statistical Mechanics. *Journal of Mathematical Physics* **1965**, *6* (10), 1447−1461. (acccessed 9/27/2024).
(20) Leven, I.; Hao, H.; Tan, S.; Guan, X.; Penrod, K. A.; Akbarian, D.; Evangelisti, B.; Hossain, M. J.; Islam, M. M.; Koski, J. P.; et al. Recent Advances for Improving the Accuracy, Transferability, and Efficiency of Reactive Force Fields. *J. Chem. Theory Comput.* **2021**, *17* (6), 3237−3251.
(21) Ue, M.; Mori, S. Mobility and Ionic Association of Lithium Salts in a Propylene Carbonate-Ethyl Methyl Carbonate Mixed Solvent. *J. Electrochem. Soc.* **1995**, *142* (8), 2577.
(22) (a) Gao, H.; Yan, Q.; Holoubek, J.; Yin, Y.; Bao, W.; Liu, H.; Baskin, A.; Li, M.; Cai, G.; Li, W.; et al. Enhanced Electrolyte Transport and Kinetics Mitigate Graphite Exfoliation and Li Plating in Fast-Charging Li-Ion Batteries. *Adv. Energy Mater.* **2023**, *13* (5), No. 2202906. (b) Kang, G.; Zhong, G.; Ma, J.; Yin, R.; Cai, K.; Jia, T.; Ren, X.; Yu, K.; Qin, P.; Chen, Z.; et al. Weakly solvated EC-free linear alkyl carbonate electrolytes for Ni-rich cathode in rechargeable lithium battery. *iScience* **2022**, *25* (12), No. 105710.
(23) Alamdar, S.; Zarif, M. Exploring lithium salt solution in sulfone and ethyl acetate-based electrolytes for Li-ion battery applications: a molecular dynamics simulation study. *Journal of Materials Chemistry A* **2024**, *12* (28), 17471−17482. 10.1039/D4TA00855C.
(24) Dhananjay; Mallik, B. S. Cage Dynamics-Mediated High Ionic Transport in Li-O2 Batteries with a Hybrid Aprotic Electrolyte: LiTFSI, Sulfolane, and N,N-Dimethylacetamide. *J. Phys. Chem. B* **2023**, *127* (13), 2991−3000.
(25) Kirkwood, J. G.; Boggs, E. M. The Radial Distribution Function in Liquids. *J. Chem. Phys.* **1942**, *10* (6), 394−402. (acccessed 9/27/2024).
(26) Pinson, D.; Zou, R. P.; Yu, A. B.; Zulli, P.; McCarthy, M. J. Coordination number of binary mixtures of spheres. *J. Phys. D: Appl. Phys.* **1998**, *31* (4), 457.
(27) Hui, S.; Roller, J.; Yick, S.; Zhang, X.; Decès-Petit, C.; Xie, Y.; Maric, R.; Ghosh, D. A brief review of the ionic conductivity enhancement for selected oxide electrolytes. *J. Power Sources* **2007**, *172* (2), 493−502.
(28) Kowsari, M. H.; Fakhraee, M. Influence of Butyl Side Chain Elimination, Tail Amine Functional Addition, and C2Methylation on the Dynamics and Transport Properties of Imidazolium-Based [Tf2N−] Ionic Liquids from Molecular Dynamics Simulations. *Journal of Chemical & Engineering Data* **2015**, *60* (3), 551−560.
(29) (a) Yeh, I.-C.; Hummer, G. System-Size Dependence of Diffusion Coefficients and Viscosities from Molecular Dynamics Simulations with Periodic Boundary Conditions. *J. Phys. Chem. B* **2004**, *108* (40), 15873−15879. (acccessed 2024/12/08). (b) Maginn, E. J.; Messerly, R. A.; Carlson, D. J.; Roe, D. R.; Elliot, J. R. Best Practices for Computing Transport Properties 1. Self-Diffusivity and Viscosity from Equilibrium Molecular Dynamics [Article v1.0]. *Living J. Comput. Mol. Sci.* **2018**, *1* (1), 6324.
(30) (a) Diederichsen, K. M.; Terrell, R. C.; McCloskey, B. D. Counterion Transport and Transference Number in Aqueous and Nonaqueous Short-Chain Polyelectrolyte Solutions. *J. Phys. Chem. B* **2019**, *123* (50), 10858−10867. (b) Fong, K. D.; Self, J.; Diederichsen, K. M.; Wood, B. M.; McCloskey, B. D.; Persson, K. A. Ion Transport and the True Transference Number in Nonaqueous Polyelectrolyte Solutions for Lithium Ion Batteries. *ACS Central Science* **2019**, *5* (7), 1250−1260. (c) Valøen, L. O.; Reimers, J. N. Transport Properties of LiPF6-Based Li-Ion Battery Electrolytes. *J. Electrochem. Soc.* **2005**, *152* (5), A882.
(31) Duangdangchote, S.; Phattharasupakun, N.; Chomkhuntod, P.; Chiochan, P.; Sarawutanukul, S.; Tomon, C.; Joraleechanchai, N.; Sawangphruk, M. Effect of fluoroethylene carbonate on the transport property of electrolytes towards Ni-rich Li-ion batteries with high safety. *Chem. Commun.* **2021**, *57* (55), 6732−6735. 10.1039/D1CC02120F.
(32) Borodin, O.; Suo, L.; Gobet, M.; Ren, X.; Wang, F.; Faraone, A.; Peng, J.; Olguin, M.; Schroeder, M.; Ding, M. S.; et al. Liquid Structure with Nano-Heterogeneity Promotes Cationic Transport in Concentrated Electrolytes. *ACS Nano* **2017**, *11* (10), 10462−10471.
(33) Fong, K. D.; Self, J.; McCloskey, B. D.; Persson, K. A. Onsager Transport Coefficients and Transference Numbers in Polyelectrolyte Solutions and Polymerized Ionic Liquids. *Macromolecules* **2020**, *53* (21), 9503−9512.
(34) Saitoh, K. I.; Takai, Y.; Sato, T.; Takuma, M.; Takahashi, Y. Optimization of LIB Electrolyte and Exploration of Novel Compounds via the Molecular Dynamics Method. *Batteries* **2022**, *8* (3), 27.
(35) (a) Borodin, O. Polarizable Force Field Development and Molecular Dynamics Simulations of Ionic Liquids. *J. Phys. Chem. B* **2009**, *113* (33), 11463−11478. (b) Bedrov, D.; Piquemal, J.-P.; Borodin, O.; MacKerell, A. D., Jr.; Roux, B.; Schröder, C. Molecular Dynamics Simulations of Ionic Liquids and Electrolytes Using Polarizable Force Fields. *Chem. Rev.* **2019**, *119* (13), 7940−7995. (c) Unke, O. T.; Chmiela, S.; Sauceda, H. E.; Gastegger, M.; Poltavsky, I.; Schütt, K. T.; Tkatchenko, A.; Müller, K.-R. Machine Learning Force Fields. *Chem. Rev.* **2021**, *121* (16), 10142−10186.

https://doi.org/10.1021/acsomega.4c08854
ACS Omega 2025, 10, 2141−2149